

Physically based ground motion prediction and validation: a case study medium-size magnitude Marmara Sea earthquakes

A. Mert¹

Received: 10 November 2016 / Accepted: 11 November 2017 / Published online: 17 November 2017
© Springer Science+Business Media B.V., part of Springer Nature 2017

Abstract The evaluation of realistic time histories for various locations around Marmara Region is aimed to provide reliable input for performance-based seismic design, hazard or risk management studies and developing new seismic standards. The applicability of empirical Green's functions methodology and physics-based solution of earthquake rupture have been assessed in terms of modeling complex geologic structures. This paper has two main objectives. The first one is to simulate five medium-size magnitude earthquakes ($M_w \approx 5.0$) recorded in the Marmara Region. A series of synthetic ground motion waveforms for three components are evaluated with a 'physics-based' solution of earthquake rupture. The simulation methodology is based on the studies of Hutchings and Wu (J Geophys Res 95:1187–1214, 1990), Hutchings (Seismol Soc Am 81:88–121, 1991; Seismol Soc Am 84:1028–1050, 1994), Hutchings et al. (Geophys J Int 168:569–680, 2007), and Scognamiglio and Hutchings (Tectonophysics 476:145–158, 2009). For each earthquake, we calculate synthetic seismograms by using 500 different rupture scenarios that are generated by Monte Carlo method for a selection of parameters within a range based on prior knowledge of where the earthquakes will occur. The second objective is to validate synthetic seismograms with real seismograms. To improve the credibility of synthetic seismograms from an engineering point of view, the methodology presented by Anderson (in 13th world conference on earthquake engineering, Vancouver, 2003) is followed. This methodology proposes a similarity score based on averages of the quality of fit measuring ground motion characteristics and uses a suite of measurements. In order to compute goodness of fit, ten different ground motion parameters were compared on a scale from 0 to 100, where 100 means perfect agreement. Because the methodology produces source- and site-specific synthetic ground motion time histories, and the goodness-of-fit scores of obtained synthetics are between 'good' and 'excellent' range (61.128–82.164) based on the

✉ A. Mert
mertay@boun.edu.tr

¹ Kandilli Observatory and Earthquake Research Institute, Boğaziçi University, Cengelkoy, Istanbul, Turkey

Anderson's score, we conclude that it can be used to produce reliable ground motion time histories for seismic risk regions to develop or improve seismic codes and standards.

Keywords Simulation of strong ground motion · Empirical Green's function · Quantitative measure goodness of fit of synthetic seismograms · Marmara Sea earthquakes

1 Introduction

Because of the increasing awareness of earthquake threat in the Marmara Region, the need for seismic hazard studies has become progressively more important for planning risk reduction actions. Earthquake hazard in the Marmara Region has been studied by probabilistic methods (Atakan et al. 2002; Erdik et al. 2004). Together with these earthquake hazard assessment studies, some researchers tried to model the bedrock ground motions in the Marmara Region using hybrid broadband simulation technique (Pulido et al. 2004; Sørensen et al. 2007; Ansal et al. 2009; Tanircan 2012). Pulido et al. (2004) combined deterministic simulation of seismic wave propagation at low frequencies with a semi-stochastic procedure for the high frequencies to model bedrock broadband ground motions in the Marmara Region. Sørensen et al. (2007) also used the same hybrid model, semi-stochastic procedure for the high frequency and deterministic model for the low frequency, to evaluate the influence of source and attenuation parameters on the simulated ground motion. Ansal et al. (2009) tried to develop earthquake loss scenarios in terms of building damage and casualties for Istanbul from computed synthetic time series of ground motion by using hybrid stochastic–deterministic approach. Tanircan (2012) combined a finite difference algorithm with three dimensional velocity structures for low-frequency simulations and a stochastic algorithm for high-frequency simulations. She obtained three different scenarios with the hybrid simulation of ground motions for Istanbul as a result of $M_w = 7.2$ earthquake on the Prince Island segment. Another hybrid strong ground motion simulation study was conducted on Prince Island segment by Mert et al. (2014a), which investigates the effects of different earthquake source parameters on the amplitude and frequency content of the simulated wave forms. This study also used finite difference algorithm to get low-frequency simulation of ground motion and physically based empirical Green's function (EGF) method for the high frequency of simulation.

Because high-frequency ground motions strongly affected by heterogeneity, high-frequency simulation algorithms based on one or more dimensional velocity structure models can produce unrealistic results, especially for regions as Marmara Region that have heterogeneous crustal structure. The results are strongly based on the reliability of velocity structure. In the literature, uncertainties due to heterogeneous structure of the Marmara Region and their effects on high-frequency ground motion simulations have not been studied. These effects significantly alter the amplitudes of seismic energy and can cause focusing and scattering. Recently, researchers (Hutchings and Wu 1990; Hutchings 1991, 1994; Jarpe and Kasameyer 1996; Hutchings et al. 2007; Scognamiglio and Hutchings 2009) attempted to model these affects by applying 'physically based' rupture process that utilizes EGF. Hartzell (1978) and Wu (1978) introduced the concept of using EGFs, and numerous methodologies were developed based on the suggested principles (Irikura 1983; Wennerberg 1990; Hutchings and Wu 1990; Frankel 1995). EGFs are used to obtain not only the effect of the free surface and attenuation of wave forms, but also

refractions, reflections and scattering due to heterogeneities along the propagation path. In addition, EGFs inherently include linear site response at the site where they are recorded.

The first main objective of this study is to evaluate realistic ground motion time histories for various locations around Marmara Region. It is aimed to provide necessary input for engineering design, retrofiting of the existing structures, hazard or risk management studies and developing new seismic standards. To use synthetic seismograms as input in engineering design purposes, first the ground motion simulation algorithms must be validated (Mert et al. 2014b). The second objective is to validate ground motion simulation algorithm. Validation procedure is not simple due to the difficulties in the determination of credible synthetic seismogram and the reliability of ground motion simulation tools. The best way to validate simulation procedure is to compare synthetic seismograms with real recorded earthquakes. At this point, there are two important questions to answer: The first question is how to determine comparison parameters, and the second one is how to decide the criteria of what a good agreement or a poor agreement is. The choice of right parameter set and identification of acceptable agreement threshold is not easy even within the civil engineering design context as explained in detail by the Euroseistest Verification and Validation Project (E2VP).

There has not been a study that was prepared in Marmara Region to validate synthetic seismograms with real seismograms from an engineering point of view. In this paper, to compare synthetic seismograms with real seismograms five medium-size magnitude earthquakes ($M_w \approx 5.0$) recorded in the Marmara Region are simulated. Simulated ground motion time histories for three components along the fault segments for a fixed magnitude are synthesized up to 25 Hz. To generate randomly varying independent rupture parameters and to include as much rupture scenarios as possible, 500 different rupture scenarios were generated by Monte Carlo method. A ‘physics-based’ solution of earthquake rupture is applied based on the studies of Hutchings and Wu (1990), Hutchings (1991, 1994), Hutchings et al. (2007) and Scognamiglio and Hutchings (2009) to obtain three components synthetic seismograms from each rupture scenarios. To improve credibility of synthetic seismogram from an engineering point of view and validate the simulation procedure, the methodology presented by Anderson is followed (2003).

2 Tectonic settings, seismicity and lithospheric structure of the Marmara Region

According to Yılmaz et al. (2009), the most prominent morphotectonic entity in the Marmara Region is the Marmara Sea, and the main morphological difference between the regions to the north and south of the Marmara Sea Basin is mainly related to the NAFZ (Fig. 1). NAFZ cuts across the Anatolian Peninsula in the E–W direction, entering into the Marmara Region and extending to the Aegean Sea (Yılmaz et al. 2009). Based on previous studies, it can be clearly stated that NAFZ creates tectonic boundary between the Anatolian and the Eurasian Plates and causes the westward movement and counterclockwise rotation of the Anatolian Plate relative to the Eurasian Plate (McKenzie 1972; Dewey and Sengor 1979; McClusky et al. 2000; Gulen et al. 2002; Horasan et al. 2002). Because, NAFZ that is the northern plate boundary of the Anatolian Plate and the N–S extensional regime of the Aegean Region intersect, tectonically region is complex and critical (Yılmaz et al. 2009). NAFZ consists of mainly a single strand between the Karlova triple junction and the Mudurnu Valley. In the eastern part of the Marmara Region, it splays into two main

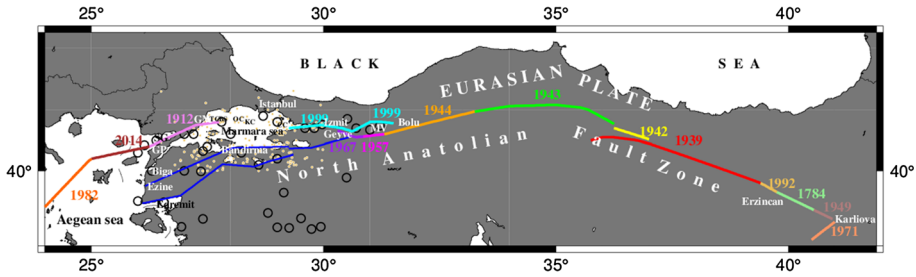


Fig. 1 The 1600-km-long NAFZ and the seismicity of the Marmara Region (in figure *TC* Tekirdag Basin, *BS* West Ridge, *KC* Kumburgaz Basin, *OC* Middle Marmara Basin, *CC* Cincarcik Basin, *MV* Mudurnu Valley, *SG* Saors Fulf, *GP* Gelibolu Peninsula, *GM* Ganos Mountains)

branches around Bolu and then into three branches around Geyve-Adapazarı (Barış et al. 2005) (Fig. 1). Regional geodetic (Reilinger et al. 1997; McClusky et al. 2000) and seismotectonic studies (Canitez and Uçer 1967; Taymaz et al. 1991; Eyidoğan et al. 1998) to estimate the rate of lateral displacement along the NAFZ close to the western end, in the Marmara Region, reveal that slip rate of the NAFZ is ranging from 17 to 24 mm/year (Barış et al. 2005).

Recalling the recent history about the NAFZ, a series of large earthquakes started in 1939 near Erzurum and propagated westward toward the Marmara Region located in northwestern Turkey where two major earthquakes, namely Izmit and Duzce–Bolu, occurred in 1999. During this period, NAFZ experienced an exceptional seismic moment release cycle rupturing the entire 1600-km-long fault zone except two segments: one beneath the Marmara Sea and the other further in the west beneath the northern Aegean Sea. On May 24, 2014, at 09:24 GMT a strong earthquake with $M_w = 6.9$ occurred in northeastern Aegean Sea, located between Gökçeada, Samothraki and Limnos islands. The 2014 event (May 24, 2014, at 09:24 GMT $M_w = 6.9$ northeastern Aegean Sea earthquake) filled one of those seismic gaps leaving only the Marmara Sea faults unruptured (Fig. 1).

The location of the NAFZ and the seismic moment release phase associated with major earthquakes is demonstrated in Fig. 1. In figure, the surface rupture extent and the date of the events are shown in different colors. Segmentation compiled from Sengör (1979), Barka and Kadinsky-Cade (1988), Armijo et al. (2002), Kurtuluş and Canbay (2007). Yellow circles are $4.0 < M < 6.0$ earthquakes from 1900 to 2014 in the Marmara Region based on BU-KOERI database. For the instrumental period, earthquake activity in the region shows typical swarm-type activities. Black circles are $M > 6.0$ earthquakes (1509–1999) based on Kalkan et al. (2009). Kalkan et al. (2009), by using the earthquake catalogs including the events from historical and instrumental seismicity, depict the distribution of all distinct events larger than magnitude 6 ($M \geq 6.0$) after the year 1500. The number of earthquakes identified in this region for the historical period is around 600. Thirty-eight of them are estimated to be relatively large shocks of magnitude $M_s \geq 7.0$ (Ambraseys and Finkel 1991). The most remarkable fact is that seven of these magnitude 7 earthquakes ($M \geq 7.0$) occurred during the last century.

During the last decades, several seismological studies were carried out in the Marmara Region to reveal velocity structure of the crust and upper mantle in order to investigate the heterogeneous structures of seismogenic zones. To determine crustal structure, travel times from local earthquakes were used by Canitez (1962) and Crampin and Ucer (1975); also a quarry blast test was conducted along a profile between Adapazarı and Osmaniye by

Gurbuz et al. (1980). Horasan et al. (2002) simulated the waveforms of the Izmit earthquake aftershocks, to determine the lithospheric structure of the Gulf of Izmit in Marmara Region. Zor et al. (2006) studied the crustal structure of eastern Marmara Region by applying teleseismic receiver function. Kuleli (1992) attempted a tomography of *P* wave velocity for the deeper structure of the Aegean Sea region including the western part of the Marmara Sea. Nakamura et al. (2002) used passive source tomography to resolve a 3D velocity structure for the Kocaeli Region and its vicinity. Karabulut et al. (2003) presented a 2-D tomographic seismic velocity image in the eastern Marmara Region along an N-S trending seismic refraction profile. Barış et al. (2005) applied a 3-D seismic tomography inversion algorithm to arrival-time data from local seismic networks and aftershock studies in the Marmara Region. All these studies generally prove inhomogeneous sharp velocity variations that reflect geological complexities and heterogenic crustal structure in Marmara Region (Barış et al. 2005).

3 Implementing and validating earthquake synthesized methodology to the Marmara Region

3.1 Methodology

In this paper, the Green's function simulation methodology (Hutchings and Wu 1990; Hutchings 1991) together with physically based rupture parameters proposed by Hutchings et al. (2007) is used to develop realistic synthetic strong ground motions for specific sites from specific faults. By 'physically based,' we refer to ground motions synthesized with quasi-dynamic rupture models (Boatwright 1981) derived from physics, and an understanding of earthquake process as described by Hutchings et al. (2007), Scognamiglio and Hutchings (2009). EGFs are defined as recordings of effectively impulsive point source events (Hutchings and Wu 1990), and their stress drop changes are reflected only in the differences of their seismic moment. The term 'Effectively impulsive point source' refers to the observation that factors such as rise time, rupture duration or source dimension are small enough that their effect cannot be observed in the frequency band of interest (Hutchings et al. 2007).

Theoretical background and formulation are summarized in Hutchings and Wu (1990) and Hutchings (1991). The methodology has been tested several times by studying past earthquakes (Hutchings 1988, 1994; Hutchings et al. 1997, 1998, 2007; Papoulia et al. 2015; Foxall et al. 1994; Hutchings and Jarpe 1996; Jarpe and Kasameyer 1996; Wossner et al. 2002; Scognamiglio and Hutchings 2009; Mert et al. 2011). By constraining source parameters from independent studies for the 1997 Colfiorito earthquake, Scognamiglio and Hutchings (2009) showed that uncertainty bounds were reduced by a factor of almost two and the actual earthquake parameters were still described by the uncertainty bounds. Foxall et al. (1994) fixed the moment, focal mechanism solution, slip distribution and geometry from independent studies and modeled the observed strong ground motion at 26 sites. Jarpe and Kasameyer (1996) found that the standard error between observed and predicted response spectra is less than or equal to other methods for periods between 0.05 and 2.0 s and is significantly less than regression methods based on Loma Prieta strong-motion data at periods between 0.5 and 5.0 s. Mert et al. (2011) made an assessment of uncertainties and confidence level in the selection of rupture parameters.

A suite of 500 different rupture scenarios are developed for each simulated medium-size magnitude earthquakes, by randomly varying independent rupture parameters within a range of physical limits given in the literature (Wells and Coppersmith 1994; Somerville

et al. 1999). To validate the simulation algorithm and develop credibility of synthetic seismogram from an engineering point of view, the methodology presented by Anderson (2003) is followed. This methodology proposes a similarity score based on averages of the quality of fit measuring ground motion characteristics. Recognizing that ground motions are consisted of very complex time series, a single parameter to compare real and synthetic seismograms is absolutely inadequate, and Anderson's method uses a suite of measurements. Namely, the synthetics are confronted to real data by comparing the values obtained ten representative ground motion criteria: peak ground acceleration (PGA), peak ground velocity (PGV), peak ground displacement (PGD), Fourier amplitude spectrum (FAS), response spectrum (RS), arias duration (AD), arias intensity (AI), energy duration (ED), energy integral (EI) and cross correlation (CC). In order to compute goodness of fit (GOF), each criterion is compared on a scale from 0 to 10, with 10 giving perfect agreement. Considering that there are ten representative ground motion criteria, Anderson method gives a score of up to 100 to compare synthetic and real seismograms. Anderson proposed that 40 to 60 represent a 'fair' fit, 60–80 a 'good' fit and 80–100 an 'excellent' fit. We tested if the calculated seismograms match the recorded waveforms, and if our score is at 'good' to 'excellent' range for the best-fitted scenario, we then accepted that methodology was validated at least from engineering point of view.

3.2 Data

To investigate the effect of crustal inhomogeneity on the ground motion simulations, utilization of medium-size magnitude earthquakes has several advantages because their rupture process is fairly simple and their source dimensions are small enough that only one small earthquake can be used as EGF (Hutchings 1994). Synthesized seismograms are generated by using quasi-dynamic models of earthquake rupture that depends on field observations, laboratory experiment and numerical modeling for five main events occurred

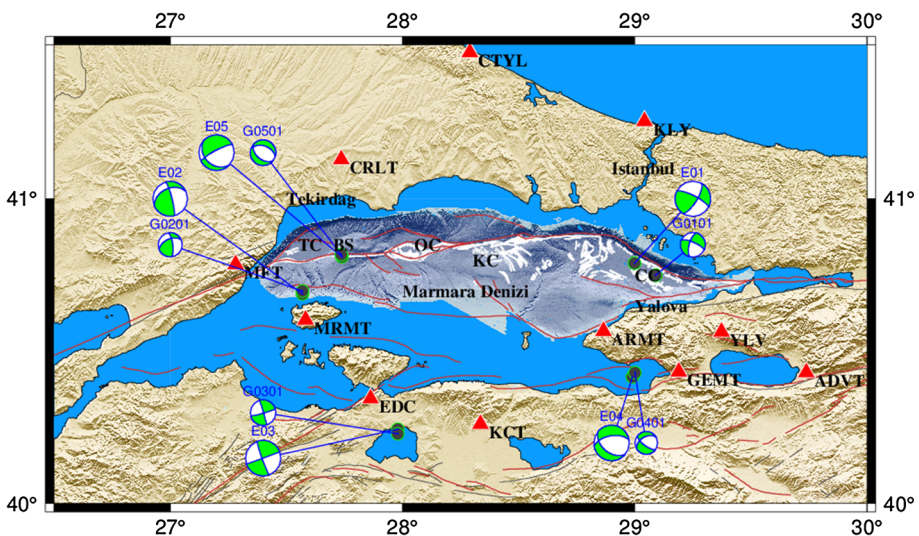


Fig. 2 Five simulated main earthquakes (green circles) and aftershocks used as an EGF (green circles) with earthquake recording network composed of broadband seismometers (red triangles) (other information on the map is same as shown in Fig. 1)

on various locations of NAFZ in the vicinity of the Marmara Sea (Fig. 2). The first main (simulated) event ($M_w = 5.0$) and its aftershock ($M_w = 3.5$) that was used as an EGF occurred on the Princes' Island fault segment, along the northern branch of the NAFZ. The second main event ($M_w = 4.9$) and its aftershock ($M_w = 3.4$) occurred north of the Marmara Island, to the south of the western segment of the NAFZ, in western Marmara Sea. Their focal mechanism calculated by moment tensor inversion algorithm reported in Pinar et al. (2003). Other two events and aftershocks occurred around Kuş Lake ($M_w = 5.0$) on the southern branch of NAFZ in the continental area of Marmara Region and on the middle branch of the NAFZ, in the Gemlik Gulf ($M_w = 5.0$), respectively. A focal mechanism solutions using moment tensor inversion algorithm for these two main earthquakes are reported by Örgülü (2011). The focal mechanism solutions for the aftershocks are calculated using first arrivals of the P waves. The last event ($M_w = 5.0$) and its aftershock ($M_w = 3.6$) occurred on the central Marmara fault which is a main extension of the northern branch of NAFZ in the Marmara Sea. Figure 2, Tables 1 and 2 describe the epicenters of all main events and aftershocks that were used as a Green's function together with recording broadband stations sites, respectively.

3.3 Determination of the source parameters

A simultaneous inversion of earthquake recordings was conducted to obtain moment (M_0), source corner frequency (f_c) and site-specific attenuation (t_g^*). Simultaneous inversion is based upon the assumption that corrected long period spectral levels, and the source corner frequencies from a particular earthquake will have the same value at each site, so that differences in spectra can be attributed to propagation path, individual site attenuation and site response (Hutchings 2004). A nonlinear least squares best fit of displacement spectra of the S-wave of the recorded seismograms were used to fit to the Brune (1970) source model to solve earthquake source parameters. The Fourier amplitude spectra of recorded seismograms were corrected to represent moment at the long period asymptote and for whole path attenuation.

We corrected spectra for the whole path attenuation (t_r^*) and solved it for site-specific attenuation (t_g^*). Corrected S-wave displacement spectra was fit to Brune (1970)

Table 1 Simulated main earthquakes and aftershocks used as EGFs

Eq ID	Date (dd.mm.yy hh:mm)	Lat (N) (°)	Long (E) (°)	Depth (km)	M_w	Location
E01	20.10.99 23:08	40.79	29.00	8	5.0	Prince Island
G0101	18.08.99 00:45	40.75	29.09	5	3.5	Prince Island
E02	20.09.99 21:28	40.69	27.57	11	4.9	Marmara Island
G0201	20.09.99 20:36	40.70	27.57	11	3.4	Marmara Island
E03	20.10.06 18:15	40.245	27.980	5.9	5.0	Kuş Lake
G0301	21.10.06 07:30	40.282	27.980	6.3	3.5	Kuş Lake
E04	24.10.06 14:00	40.417	28.990	5.7	5.0	Gemlik Gulf
G0401	03.11.06 00:20	40.431	29.001	9.2	3.2	Gemlik Gulf
E05	25.07.11 17:57	40.811	27.739	15.3	5.0	North segment
G0501	25.07.11 20:43	40.817	27.736	5.4	3.6	North segment

M_w Moment magnitude

Table 2 Broadband seismometer stations recorded main earthquakes and aftershocks used as EGFs

St Id	Location	Latitude (°)	Longitude (°)	Elevation (m)	Seismometer
ADVT	İZNİK	40.4332	29.7383	193	3ESP-DM24
ARMT	ARMUTLU	40.5683	28.8660	320	3ESP-DM24
CRLT	ÇORLU	41.1290	27.7360	230	3ESP-DM24
CTYL	ÇATALCA	41.4760	28.2897	77	3T-DM24
EDC	EDINCIK	40.3468	27.8633	257	3T-DM24
GEMT	GEMLİK	40.4350	29.1890	220	3T-DM24
KCT	KARACABEY	40.2625	28.3353	445	3ESP-DM24
KLY	KİLYOS	41.2530	29.0420	30	3T-DM24
MFT	MÜREFTE	40.7867	27.2812	924	CMG40T
MRMT	MARMARA ADASI	40.6058	27.5837	213	3T-DM24
YLV	YALOVA	40.5667	29.3728	879	3T-DM24

displacement spectral shape by fitting frequencies from 0.5 to 20 Hz for all aftershocks and 0.15 to 25 Hz for the main events. Because the whole path attenuation (t_r^*) can be different at each site in the highly heterogeneous Marmara Region (Mert et al. 2010), this inversion may lead to bias in evaluation of the corner frequency (Gök 2009) [Gok et al. solved for a combined solution of whole path and site response to account for the heterogeneity]. Figure 3 shows fits to observed spectra simultaneously for source and individual station attenuation (t_g^*). The differences in shapes of individual spectra are due to site-specific attenuation (t_g). The solid line shows the modified Brune model over the frequency band that was used in this paper. Actual moment is the projection of this fit to asymptotic low frequency. Table 3 lists the source parameters determined for the main events and event that were used as an EGF.

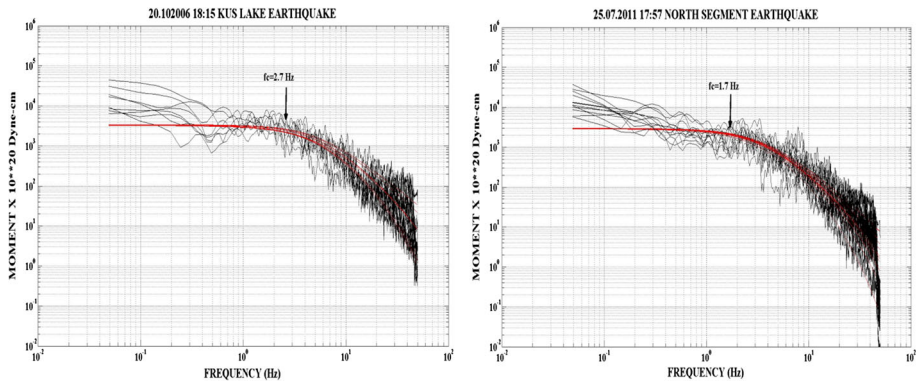


Fig. 3 Corrected spectra (black line) from each station are fitted to theoretical Brune spectra (red lines) by using simultaneous inversion for moment, source corner frequency and site-specific attenuation (t_g^*) for five main event

Table 3 Source parameters of main earthquakes and aftershocks used as EGFs

Eq id	Mechanism Stk-Dip-Rake	M_w	M_0 (dyn cm)	f_c (Hz)	Number of Stn
E01	32 71 16	5.0	$0.356 \pm 0.082 \times 10^{24}$	0.9	4
G0101	196 66 –18	3.5	$0.432 \pm 0.199 \times 10^{22}$	6.2	4
E02	245 40 166	4.9	$0.307 \pm 0.170 \times 10^{24}$	2.0	5
G0201	246 51 156	3.4	$0.197 \pm 0.105 \times 10^{22}$	9.2	5
E03	68 75 –147	5.0	$0.3431 \pm 0.201 \times 10^{24}$	2.7	8
G0301	74 86 –177	3.5	$0.191 \pm 0.014 \times 10^{22}$	8.2	5
E04	127 62 –49	5.0	$0.352 \pm 0.089 \times 10^{24}$	1.7	8
G0401	118 69 –42	3.2	$0.802 \pm 0.083 \times 10^{21}$	7.0	4
E05	242 79 –119	5.0	$0.303 \pm 0.062 \times 10^{24}$	1.7	12
G0501	130 47–75	3.5	$0.322 \pm 0.114 \times 10^{22}$	5.0	5

M_w Moment magnitude, M_0 Seismic moment, f_c Source corner frequency

3.4 Synthetic rupture models for simulated earthquakes

To identify rupture process of an earthquake, the ultimate solution would be dynamic solutions that have known elastic constants and constituent relations that satisfy elastodynamic equation of seismology and fracture energy. However, these parameters are very uncertain in the fault rupture area, and several poorly bounded assumptions were used in the literature to identify them. In this study, rupture models are consistent with the elastodynamic equation of seismology and fracture energy, and with a physical understanding of how earthquakes rupture as explained in Hutchings et al. (2007).

Rupture parameters used to create rupture scenarios were selected randomly. Range of physical limits of rupture parameters was obtained from the literature (Wells and Coppersmith 1994; Somerville et al. 1999). Moment is fixed for a particular set of rupture scenarios. Rise time, stress drop and energy are dependent variables. In different models, the high-frequency variability is due to short wavelength (asperities), or short time duration (rise times and roughness variability), and longer scale changes due to focal mechanism radiation variation or long-scale-length finite fault effects, such as directivity and moment distribution which also cause a variability in the low-frequency range as explained Hutchings et al. (2007).

During analysis, to determine certain conditions such as fault geometry, fault plane length and width or range of source parameters such as rupture velocity, roughness and location of hypocenter, many runs were performed. To cover whole segment and to calculate hazard along whole fault segment, the length of fault plane was selected to be 25 km and midpoint of length was taken as the original calculated hypocenter for each simulated earthquake. The width of fault plane was selected to be 15 km. Fault plane is different from the fault rupture area and can be described as the total area of all 500 different earthquake simulations. Namely, for each earthquake scenario the location of hypocenter and the fault rupture area were relocated or shifted inside of the fault plane. The fault rupture area was discretized into 0.01 km^2 elemental areas, which are small enough to model continuity of the rupture for frequencies up to $f \leq 25 \text{ Hz}$. The rupture initiates at the hypocenter and propagates radially at a certain fraction of the shear wave velocity. Kostrov healing model (Kostrov 1964) is used to calculate the slip at any point; we approximate the shape of the

model as a ramp function. The velocity model is used for synthesis of a linearly increasing velocity model that approximates the discrete layer model of Karabulut et al. (2003) over a 5–30 km depth range and a $v_p = 0.0788z + 5.4$ with a half-space of 8 km/s at 33 km. The depth of the upper edge of the fault planes was set to 5 km, to avoid slip at the ground surface.

The modeling parameters and the range of their values, used for the five medium-size magnitude earthquakes, are summarized below

Moment was calculated for all the main events and also for the small magnitude earthquakes used as empirical Green's functions. The value of the moment and the corresponding moment magnitudes, given in Table 3, were calculated according to the Hanks and Kanamori relation (1979). The calculated moments change between $0.303 \pm 0.062 \times 10^{24}$ and $0.356 \pm 0.082 \times 10^{24}$ dyn cm, and corresponding moment magnitude is $M_w = 5.0$ for the main events. For small magnitude earthquakes which used as EGF, the moments change between $0.802 \pm 0.083 \times 10^{24}$ and $432 \pm 0.199 \times 10^{24}$ dyn cm and corresponding to a moment magnitude range between $M_w = 3.2$ and $M_w = 3.5$.

Hypocenter locations of the simulated events were changed randomly along the fault plane

Strike, rake, dip are selected based on focal mechanism solutions of five simulated earthquake and variation range determined considering geometrical spreading of NAFZ segments in the vicinity of Marmara Sea.

Fault rupture geometry of the faults is constrained to be rectangular. The rupture area varies from 4 to 9 km² for the studied 500 different earthquake scenarios. Moment and fault rupture area are two parameters significantly affect the slip amplitudes.

Rupture velocity is not fixed, but in general for all of the different earthquake scenarios it varies from 0.75 to 1.0 times shear wave velocity.

Healing velocity is not fixed, but in general it varies from 0.8 to 1.0 times the rupture velocity for all of the different earthquake scenarios. This is the range roughly between the Rayleigh and shear wave velocities. The healing velocity is the velocity for the stress pulse that terminates slip and initiates after the rupture arrives at any fault edge.

Rise time is equal to the time it takes, after the initiation of rupture, for the first healing phase to arrive. In other words, it is the shortest time for the rupture front to reach to an edge and a healing pulse to return to the element.

Roughness is simulated as the elements resisting rupture and then breaking. A varying percentage of elements (0, 10, 33 or 50%) have a shortened rise times between 0.1 and 0.9 times the original value or those of neighboring elements, but with rupture completed at the same time. This will distribute randomly on the fault because of the radial arrangement of elements. A fixed value (33%) was assumed as roughness for these elements for all the studied scenarios, corresponding to a high stress drop.

Stress drop is a dependent variable derived from the Kostrov slip function and allowed to vary due to two other effects modeled in rupture. The first asperities are allowed to have different stress drops than surrounding portions of the fault. Second stress drop is constrained to diminish near the surface of the earth. In this study, because simulated earthquakes are medium-size magnitude earthquakes, rupture never reach to the surface. Stress drop is a significant parameter that affects the amplitudes of the simulation results.

One another important argument in this study is that a prediction is tried to be made for the range of ground motions that may occur from an earthquake at a particular magnitude within a source zone or along a fault. In Fig. 4b, the variations of mean PGA, mean PGV, mean ln (PSA), mean AAR (at 0.2 s) and mean AAR (at 1.0 s) are plotted as a function of

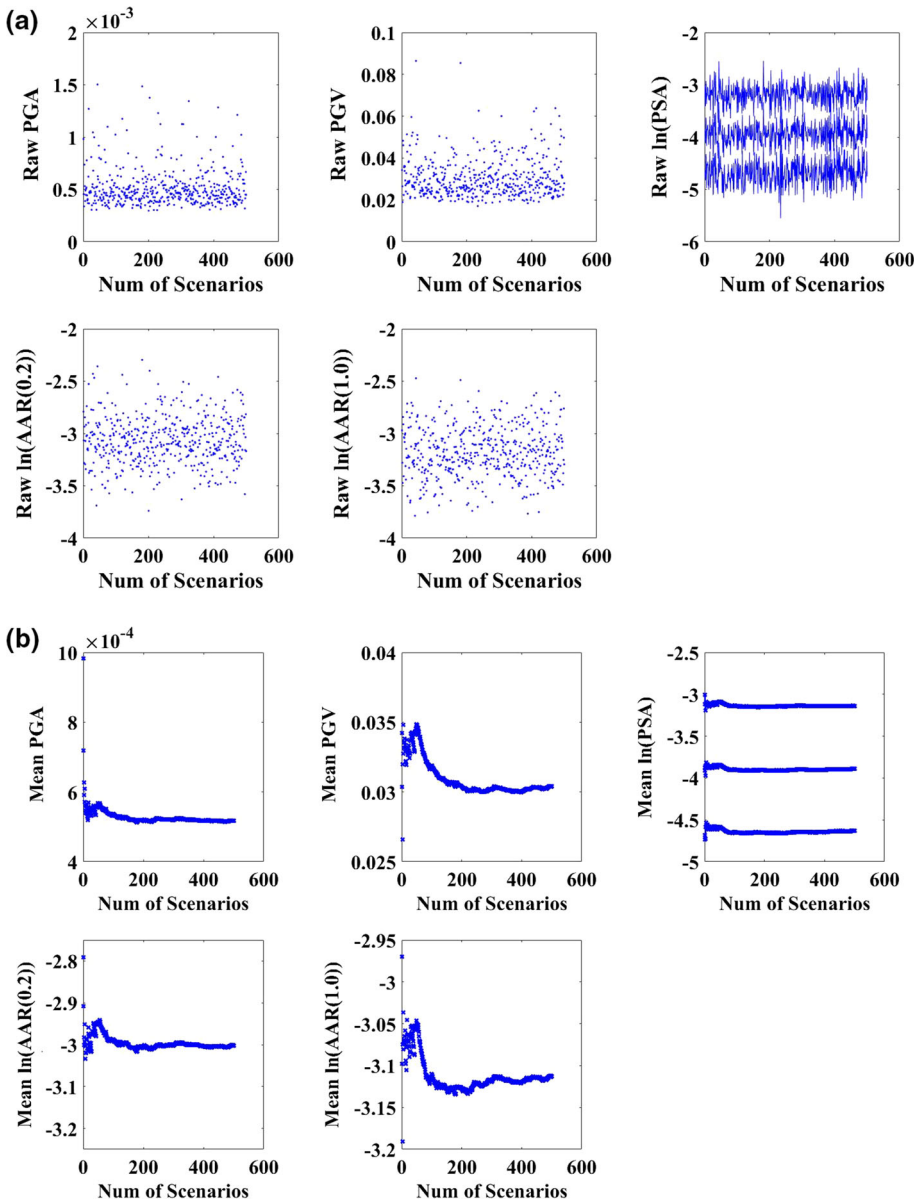


Fig. 4 **a** Variability of PGA, PGV, ln(PSA), AAR at 0.2 s and AAR at 1.0 s values (raw results) obtained from 500 different scenarios based on Kus Lake earthquake (St: KLY Comp: E-W) simulations. **b** Variability of mean PGA, mean PGV, mean ln(PSA), mean AAR at 0.2 s and mean AAR at 1.0 s as a averaged over the number of scenarios calculated based on Kus Lake earthquake (St: KLY Comp: E-W) simulations

number of scenarios. Namely, if we consider PGA, for the 10th scenario, ten different PGA values were obtained from ten different earthquake simulations and their mean was considered and plotted versus the 10th scenario. The same procedure was applied for all other

500 scenarios. After about 100 scenarios of all calculated parameters, stabilization of the means was realized, indicating that 500 models span the full variability of ground motion and effectively constrains the range of prediction. The variability functions for the different stations for all simulated earthquakes are checked and the same results were concluded.

4 Results

4.1 Simulation of five medium-size magnitude earthquakes

All the modeled earthquakes and their aftershocks that occurred on three different main branches of the NAFZ in the vicinity of Marmara Sea have well-constrained hypocenters, focal mechanism solutions, source corner frequency and moments. Simulated and real-time histories and spectrums for two horizontal components are provided for four or five recording stations. The distance between earthquakes and the recording stations varies from 9.1 to 152.6 km, and the distance between simulated earthquake and its EGF varies from 1.1 to 8.73 km. Figure 5 illustrates modeled fault geometry and slip distribution on rectangular rupture plane for five main earthquakes based on best-fitted scenario.

Table 4 explains the studied rupture model parameters based on best scenario for five simulated earthquakes. Those results are consistent with the source rupture process of similar size earthquakes. The source characterization and slip history of Gemlik and Kus Lake earthquakes was studied in Bekler et al. (2010). They performed waveform inversions for the frequency range of 0.1–0.5 Hz using the multiple time window linear waveform inversion methodology to investigate the source size and final slip model of these two earthquakes but did not yield a non-unique solution. For that reason, they analyzed various rupture models until both observed and synthetic data were matched. Their results indicate average slip 34 cm and seismic moment 0.155×10^{24} dyn cm for Gemlik earthquake and 32 cm and 0.149×10^{24} dyn cm for Manyas earthquake. In this study, seismic moment of these two earthquakes is calculated to be two times larger than their results. The average slip value based on best-fit scenario is 30 cm for Gemlik earthquake and 23 cm for Kus Lake earthquake in this study. Unfortunately, there is no any other study in the literature that was studied to determine source rupture process specifically for other three simulated earthquakes, but these parameters seem quite compatible for moderate size earthquake

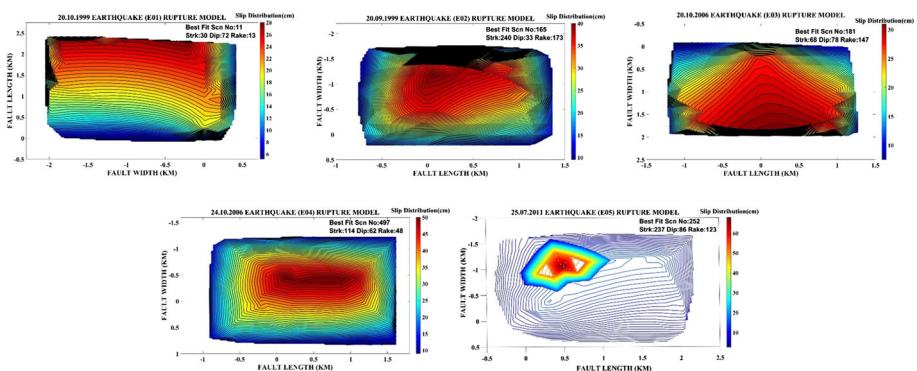


Fig. 5 Rupture models and slip distributions within rectangular rupture planes for five simulated event in and around Marmara Sea (slip distributions based on best-fit scenario earthquake)

Table 4 Comparison of real and simulated earthquakes source parameters

Earthq	Location (R)		Location (S)		M_0 ($\times 10^{24}$)	M_0 (R) ($\times 10^{24}$)	M_0 (S) ($\times 10^{24}$)	RA (km ²)	AS (cm)	RV (% V_s)	HV (% V_r)	SD (Bar)	FD (sn)	SV (cm/s)	RT (sn)
	N	E	N	E											
E01	40.79	29.00	40.796	29.024	7.54	0.3561 + 0.0829	0.4	6.6	18.5	0.86	0.94	226.9	1.19	299.9	0.07
E02	40.69	27.57	40.694	27.529	12.32	0.3069 + 0.1699	0.5	4.6	25.8	0.97	0.85	140.4	0.84	170.6	0.17
E03	40.24	27.98	40.224	27.944	10.94	0.3431 + 0.2007	0.5	5.5	22.9	0.99	0.95	187.5	0.76	219.6	0.11
E04	40.42	28.99	40.390	29.015	8.51	0.3516 + 0.0886	0.5	5.6	30	0.96	1.0	100.9	0.78	166.9	0.23
E05	40.81	27.74	40.841	27.775	20.39	0.3025 + 0.0621	0.4	5.6	13.1	0.90	0.83	69.9	0.90	96.03	0.15

R Real S simulated M_0 moment RA rupture area AS average slip RV rupture velocity HV healing velocity SD stress drop FD faulting duration SV slip velocity RT rise time

source dimension and rupture process in the literature (Wells and Copersmith 1994; Somerville et al. 1999).

4.2 Validation of synthetic seismograms

Using the data set that include one EGF for each simulated earthquake, synthesized ground motions are evaluated and compared with real earthquake records. To validate methodology and develop credibility of synthetic seismogram from an engineering point of view, two different tests were applied. The first test is based on comparison of different spectral (SD, PSV, PSA, AAR and FAS) and time domain (PGA, PGV, PGD) parameters. We compare the distribution of spectral parameters, spectral displacement (SD), pseudo velocity response (PSV), pseudo acceleration response (PSA), absolute acceleration response (AAR), Fourier amplitude spectrum (FAS) calculated from the scenario earthquakes to those calculated from the recorded ground motion. These spectral parameters do not take into account Anderson procedure except FAS. For that reason, that parameter set is selected. The simulated and actual values are compared to see whether these values correspond to each other for five different stations. The present plots here are only for the Kus Lake earthquake. Figure 6 shows comparison results (frequency domain parameters) for five different stations obtained from Kus Lake earthquake that has the best Anderson score (82.164) among all five simulated earthquakes. It is clear that all spectral parameters obtained from the best-fit scenario earthquake match very well to the observed earthquake spectral parameters nearly for all of the frequency band.

We have calculated and compared time domain parameters peak ground acceleration (PGA), peak ground velocity (PGV), peak ground displacement (PGD) for all synthetic seismograms obtained from the computed scenarios and recorded earthquakes. Figure 7a, b also shows comparison results (time domain parameters) for five different stations obtained from Kus Lake earthquake. Similarities between recorded and simulated waveforms were

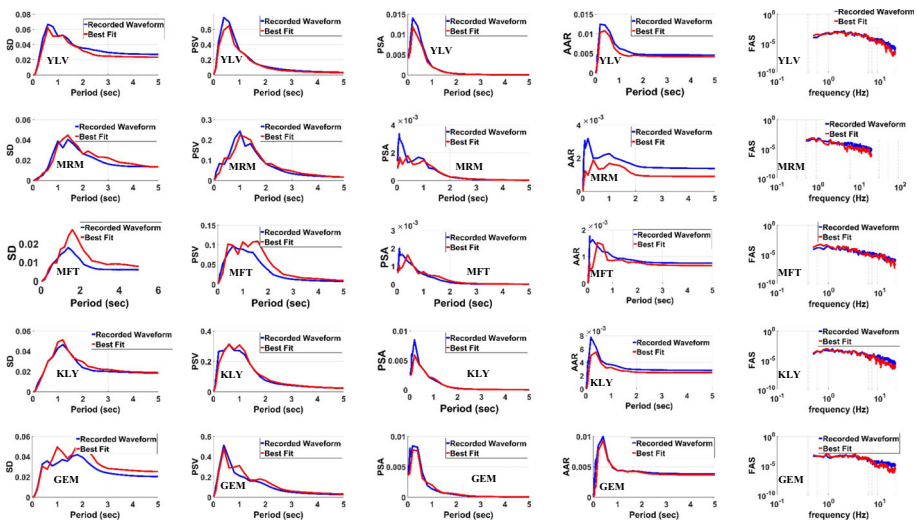


Fig. 6 Comparison of real and simulated spectral parameters (SD, PSV, PSA, AAR and FAS) for Kus Lake earthquake based on best-fitted scenario (Sc. 181). This earthquake has best Anderson score between all five simulated earthquakes

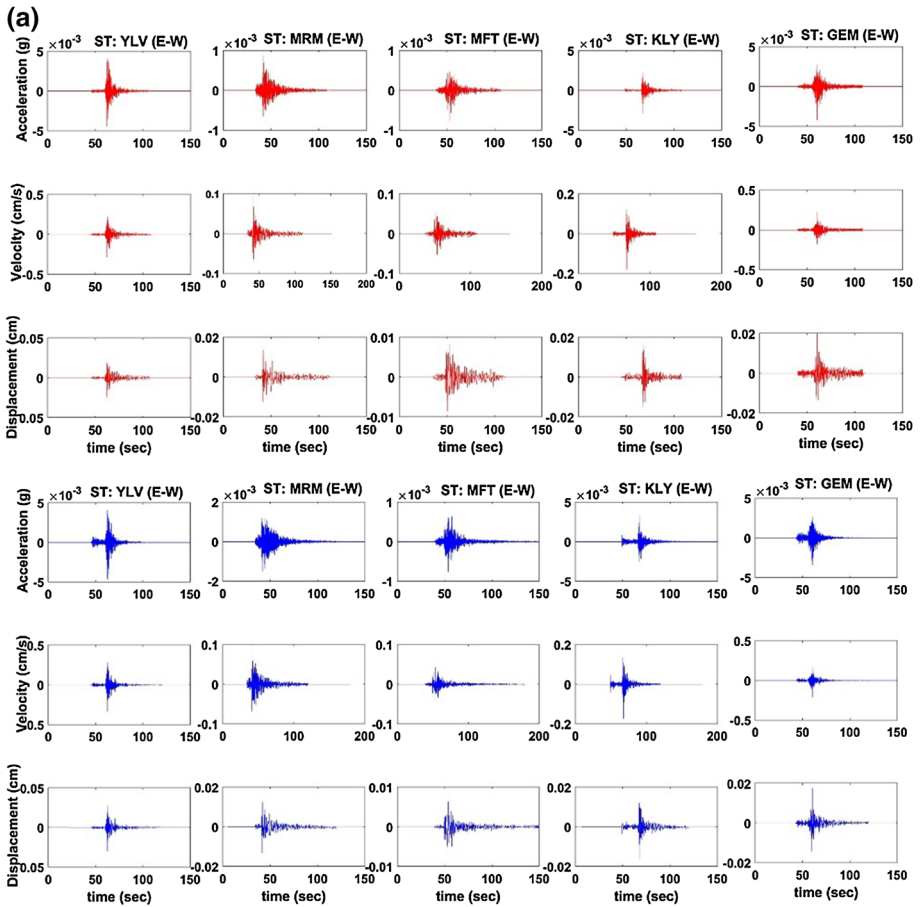


Fig. 7 **a** Comparison of real and simulated time domain parameters of Kus Lake earthquake (PGA, PGV, PGD) based on best-fitted scenarios for all five earthquakes. In figure, red solid line best-fitted simulation result and blue solid line is recorded earthquake. **b** Comparison of real and simulated time domain parameters of Kus Lake earthquake (PGA, PGV, PGD) based on best-fitted scenarios for all five earthquakes. In figure, red solid line best-fitted simulation result and blue solid line is recorded earthquake

investigated in terms of different parameters such as first arrivals of P waves, time differences between S and P wave arrivals, recording duration, maximum ground acceleration, maximum ground velocity and maximum ground displacement. The results are highly satisfactory and confirm that proposed methodology provides ground motion estimates comparable or even more realistic than those other simulation algorithm.

As a second test, an estimation is made to the quality of the fit between synthesized seismograms from each scenario earthquake and observed records. We tested that whether we can simulate seismograms that match the recorded waveforms. If the match is good or excellent, it is accepted that this scenario is close to what happened in reality during the earthquake or represent earthquake rupture process. The methodology presented by Anderson (2003) is followed, and the frequency range of the analysis for calculating Anderson’s score is 0.5–20 Hz for all criteria except response spectra. Response spectra are calculated for the period range 0.2–5 s for every 0.2 s time step. Table 5 summarizes

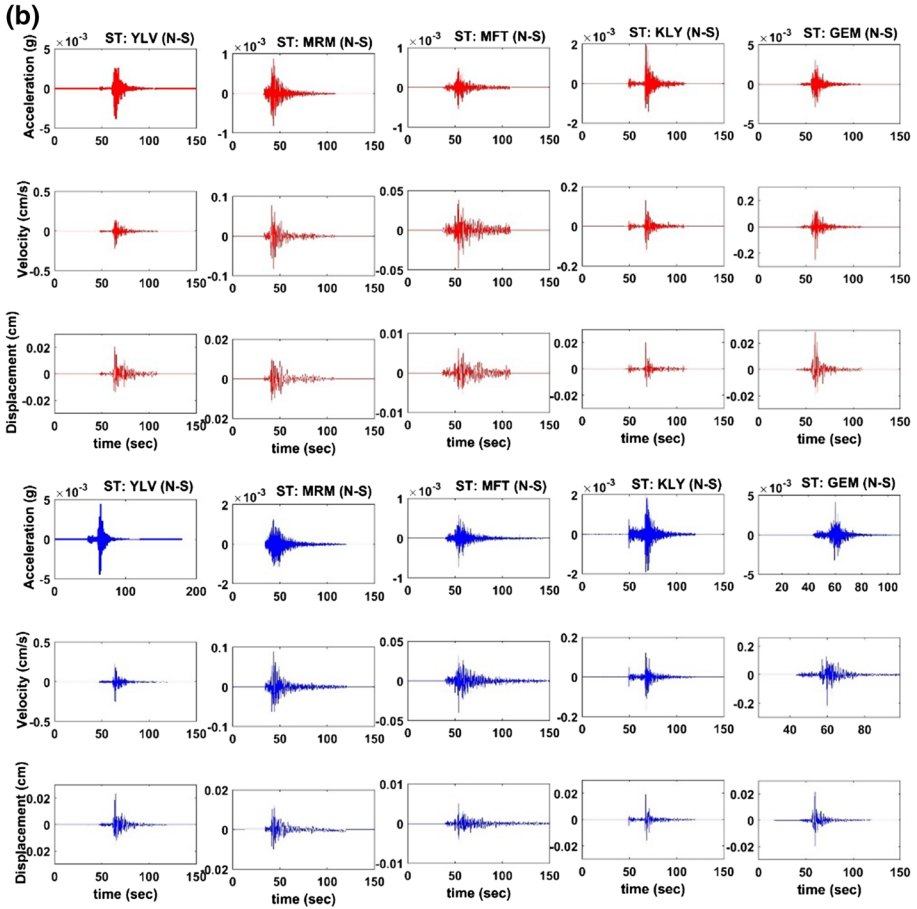


Fig. 7 continued

the results for each parameter obtained from the worst and the best Anderson score earthquake scenarios to prove the success of simulation algorithm, and eventually, Table 6 summarizes the total Anderson score obtained from the worst and the best score earthquake scenarios by using five stations for five different earthquakes

If we consider all scenario results for all stations, the first five parameters (PGA, PGV, PGD, FAS and RS) have always better score than the others. For example, if we consider only best-fit scenario results and only these five criteria, goodness-of-fit score will be always good to excellent range and mostly excellent. This proves that according to basic characteristics of ground motion simulation EGF method simulates real earthquake successfully. For the other three criteria (AI, AD, ED), scores are mostly good to excellent range. The last two criteria (EI, CC) have the worst score for all scenarios as expected.

Table 5 Comparison of different Anderson scores by using the worst and the best score earthquakes

SC NO	PGA	PGV	PGD	FAS	RS	AD	AI	ED	EI	CC	Summation	ST name
Worst score earthquake (E05)												
CEN252	9.28604	9.32452	9.86466	6.90157	9.03580	7.62402	9.88940	6.67320	1.74624	0.79519	71.14064	ARM
CEN252	9.04441	9.10460	5.62429	6.71846	6.19150	8.92650	8.97743	7.73391	2.10191	4.10327	68.52626	CRL
CEN252	6.43694	6.94085	7.09619	6.84857	8.60270	9.95627	9.71105	6.05144	3.07752	1.23993	65.96145	CTY
CEN252	7.84347	8.61967	6.18326	0.60906	1.81619	5.19538	4.14918	7.10200	2.35693	3.19820	47.07335	EDC
CEN252	8.15051	8.69489	9.50072	1.31172	4.26128	5.50028	8.35433	6.39703	0.73134	0.03419	52.93628	MRM
Best score earthquake (E03)												
KGO181	9.98026	9.93645	9.86463	8.29200	6.85717	7.93091	5.85543	8.09061	3.38393	6.80405	76.99543	GEM
KGO181	9.17308	9.29903	9.77186	9.75257	9.27533	9.55548	9.98849	8.02384	3.31154	7.01309	85.16431	KLY
KGO181	9.82432	9.67282	9.91284	8.96259	6.60601	9.49593	8.05418	7.03250	3.80191	7.06711	80.43020	MFT
KGO181	9.96728	9.90866	9.90743	9.00494	9.92443	8.65720	9.89169	7.63404	2.69640	5.54300	83.13506	MRM
KGO181	9.37576	9.40304	9.88666	7.70271	8.91755	9.48599	9.93741	8.39078	3.83788	8.15754	85.09533	YLV

Table 6 Anderson scores that were obtained the best scenario between five hundred different earthquake scenarios for five Marmara Sea earthquakes from different recording stations

Eq id	Best scenario	Anderson score	Worst scenario	Anderson score
E01	SC 11	68.468	SC 65	15.486
E02	SC 165	72.739	SC 290	8.140
E03	SC 181	82.164	SC 234	7.573
E04	SC 497	64.332	SC 108	19.974
E05	SC 252	61.128	SC 64	10.400

5 Discussion and conclusions

Simulation of high-frequency ground motion is still a difficult problem in seismology due to its random nature. Probably, the most important restriction for that kind of simulation algorithm is related to the calculation of source and propagation path characteristics. Propagation complexities are not well captured by crustal models, which provide the basis for calculation of synthetic Green's functions. At high frequencies (> 1 Hz), wave propagation is very sensitive to small crustal heterogeneities, which are generally not well known; at low frequencies (< 1 Hz), wave propagation can be modeled fairly accurately. EGFs can be used instead of mathematical calculations to more accurate representation of seismic wave propagation in the geologically heterogeneous crust. The EGF method is the best available method because it empirically corrects for unknown path and site effects, for which a short-wavelength resolution is needed. However, true EGFs contain the source rupture process of the small earthquakes in the recorded seismograms. No earthquake has a true impulsive source. Therefore, one must be careful using EGFs. Hutchings et al. (2007) demonstrated how to utilize slightly larger earthquakes ($M \cong 3$) as point sources in the solution. Other factors need also to be considered; Wossner et al. (2002) researched the effects of a limited number of Green's functions and variations in moment calculations, Hutchings and Wu (1990) researched the effects of variations in focal mechanism solutions or interpolation, and Hutchings et al. (2007) incorporated their effects into uncertainty of the solution. EGFs are theoretically from impulsive point sources, which in our application require the rupture duration of the source event to be short enough that the source corner frequency is higher than the highest frequency of interest.

Synthesizing ground motion seismograms for five medium-size magnitude earthquakes ($M_w \approx 5.0$) recorded in Marmara Region have showed that EGFs can be used to account for many of the inhomogeneity in complex geologic structure with lateral velocity variations. Using the small magnitude earthquake as an EGF together with an appropriate source function to simulate high-frequency ground motion is the most promising idea that copes with this problem. The applicability of EGFs methodology and physics-based solution of earthquake rupture had been assessed in terms of modeling complex geologic structure. This study has identified particular fault segments and earthquakes of particular moment occurred in these segments together with sufficient variations of rupture parameters. By using 500 different rupture scenarios, this methodology have tested that if a particular fault segment is identified as capable of having an earthquake of a particular moment, and if sufficient variations of rupture parameters are sampled, then the suite of

synthesized seismograms would encompass all possible seismogram that could occur from an earthquake of that moment along that fault.

This study also tested that the rupture characteristics of a fault can be constrained by range of physical parameters and the range of possible fault rupture scenarios which covers the limits of the earthquake process and effectively constrains the range of predictions. These are first three hypothesis proposed by Hutchings et al. (2007), and the results in this study support these hypothesis for highly heterogeneous Marmara Region.

To determine correct rupture parameter sets, many different trial runs have been performed. These runs have shown that using rectangular fault geometry rather than elliptical and fixing roughness to 33% produces better results. One another important issue that directly affects the simulation results is selection of small earthquake to use as an EGF. It can be concluded that signal-to-noise ratio of recorded waveforms is one of the most important parameter, but not the only one, that affects the results.

The primary reason to use 500 different rupture scenarios is due to the fact that one of them should generate synthesized seismograms that would match those that were observed. This is particularly important because it would ensure that the actual ground motion from future earthquake would be included in any application, such as performance-based design of structures. This is tested with the ‘Anderson’ score, which measures ten characteristics of strong ground motion which are important for engineered structures.

Modeling exact waveforms was not perfect for all of the stations. There are several limitations related to EGFs. The selection of an EGF follows strict criteria that are not always possible to fulfill. However, a good match to observed seismograms was obtained. It is clear that nobody expects simulated time history obtained from a simple source model and one EGF to match each cycle of the real earthquake record. The uncertainty in a ground motion simulation arises from the variability in source characteristics and from different layers of earth structures through which seismic waves propagated. The ultimate solution for modeling earthquakes would be dynamic solutions that satisfy both elastodynamic equations and fracture mechanics that have known elastic constants and constituent relations for faulting processes. Estimation of these parameters for the fault zone carries large uncertainties and requires several poorly bounded assumptions. The resultant uncertainties in computations limit their usefulness in better understanding of the earthquake process and in providing bounds for kinematic rupture models.

Because the methodology produces source- and site-specific synthetic ground motion time histories with a goodness-of-fit scores between ‘good’ and ‘excellent’ range (61.128–82.164) based on Anderson (2003), this methodology can be tried to produce ground motion that has not been recorded previously during a catastrophic earthquake in the region and it can be used to develop or improve seismic codes and standards. One another validation consisted in this study is that the method can produce synthetic seismogram from an engineering point of view which is the comparison of four different spectral parameters (AAR, PSA, PSV and SD) that match observed spectrum. The shapes of the spectral parameter curves match those of the all five earthquakes for all stations in over all periods. By using only one EGF to simulate medium-size magnitude earthquakes ($M_w \approx 5.0$), usage of single EGF is tested for this simulation approach. Previous studies tested only small earthquakes ($M_w \approx 3.5$), using single EGF, or much larger earthquakes ($M_w \approx 6$), using multiple EGFs.

As a future plan, we will estimate the seismic hazard in the Marmara Region associated with the all predetermined fault segments and we will utilize the ‘physically based probabilistic seismic hazard analysis’ (Pb-PSHA) approach proposed by Hutchings et al. (2007), Scognamiglio and Hutchings (2009). This methodology provides source- and site-

specific calculations of full-time histories. We replace empirical attenuation relationship from calculation of standard probabilistic seismic hazard analysis (PSHA) with calculation of physically based synthetic seismogram.

Acknowledgements This work was supported by the Scientific and Technological Research Council of Turkey (TÜBİTAK) under 2219 Postdoctoral Research Fellowship Programme Number: B.14.2. TBT.0.06.01-219-84, TÜBİTAK under 3501 Career Development Program Project Number: 116Y091 and Scientific Research Projects Coordination Unit of Bogazici University under Project Number 7520.

References

- Ambraseys NN, Finkel C (1991) Long-term seismicity of Istanbul and of the Marmara sea region. *Engineering Seismology and Earthquake Engineering* 91/8, Imperial College of Science and Technology
- Anderson JG (2003) Quantitative measure of the goodness of fit of synthetic accelerograms. In: 13th world conference on earthquake engineering, Vancouver, August 1–6, 2004, Paper no. 243
- Ansal A, Akıncı A, Cultera G, Erdik M, Pessina V, Tönük G, Ameri G (2009) Loss Estimation in İstanbul based on deterministic earthquake scenarios of the Marmara Sea region (Turkey). *Soil Dyn Earthq Eng* 29:699–709
- Armijo T, Meyer B, Navarro S, King G, Barka A (2002) Asymmetric slip partitioning in the Sea of Marmara pull-apart: a clue to propagation processes of the North Anatolian fault? *Terra Nova* 14:80–86. <https://doi.org/10.1046/j.1365-3121.2002.00397.x>
- Atakan K, Ojeda A, Meghraoui M, Barka A, Erdik M, Bodare A (2002) Seismic hazard in İstanbul following the 17 August 1999 Izmit and 12 November 1999 Düzce earthquakes. *Bull Seismol Soc Am* 92:466–482
- Bariş S, Nakajima J, Hasegawa A, Honkura Y, Ito A, Ucer B (2005) Three dimensional structure of Vp, Vs and Vp/Vs in the upper crust of the Marmara Region, NW Turkey. *Earth Planets Space* 57:1019–1038
- Barka AA, Kadinsky-Cade K (1988) Strike-slip fault geometry in Turkey and its influence on earthquake activity. *Tectonics* 7(3):663–684
- Bekler FN, Meral ÖN, Birgören TG (2010) The fault characteristics and the rupture model of the recent moderate earthquakes in southern marmara region. In: EGU General assembly, geophysical research abstracts, vol. 12, EGU2010-11232-2
- Boatwright JL (1981) Quasi-dynamic models of simple earthquake: an application to an aftershock of the 1975 Oroville, California earthquake. *Bull seismol Soc Am* 71:69–94
- Brune JN (1970) Tectonic stress and the spectra of seismic shear waves from earthquakes, *J Geophys Res*, 75:4997–5010, (Correction, *J Geophys Res* 76(20), 5002, 1971)
- Canitez N (1962) Gravite ve sismolojiye gore Kuzey Anadolu'da Arz kabugunun yapisi. ITU Maden Fak. Yay, İstanbul, p 87
- Canitez N, Uçer B (1967) Computer determinations for the fault plane solutions in and near Anatolia. *Tectonophysics* 4:235–244
- Crampin S, Ucer B (1975) The seismicity of Marmara Sea region of Turkey. *Geophys J R Astron Soc* 40:269–288
- Dewey JF, Sengor AMC (1979) Egean and surrounding regions: complex multi-plate and continuum tectonics in a convergent zone. *Bull Geol Soc Am* 90:84–92
- Erdik M, Demircioğlu M, Sesetyan K, Durukal E, Siyahi B (2004) Earthquake hazard in Marmara region Turkey. *Soil Dyn Earthq Eng* 24:605–631
- Eyidoğan H, Cisternas A, Gürbüz C, Aktar M, Haessler H, Türkelli N, Biçmen F, Uçer SB, Kuleli S, Barka A, Işıkara AM, Polat O, Kaypak B, Ergin M, Arpat E, Yörük A, Bariş Ş, Kalafat D, Alçık H, Güngör A, İnce Ş, Zor E, Bekler T, Gök R, Görgülü G, Kara M (1998) Marmara Denizi ve çevresindeki Mikro-deprem araştırmasının sonuçları. *Deniz jeolojisi, Türkiye Deniz Araştırmaları, Workshop-IV*, pp 13–18
- Foxall W, Hutchings L, Jarpe S (1994) Lithological and rheological constraints on fault rupture scenarios for ground motion hazard prediction. In: IUTM Symposium on Mechanics Problems in Geodynamics, Beijing, China, Sept 5–9 1994. Lawrence Livermore National Laboratory, pp 27 (UCRL-JC 116437)
- Frankel A (1995) Simulating strong motion of large earthquakes using recordings of small earthquakes: the Loma Prieta main shock as a test case. *Bull Seismol Soc Am* 85:1144–1160
- Gök R, Hutchings L, Mayeda K, Kalafat D (2009) Source parameters for 1999 North Anatolian Fault zone Aftershocks. *Pure Appl Geophys*. <https://doi.org/10.1007/s00024-009-0461-x>

- Gulen L, Pinar A, Kalafat D, Ozel N, Horasan G, Yilmazer M, Isikara AM (2002) Surface fault breaks, aftershock distribution, and rupture process of the 17 August 1999 Izmit, Turkey, earthquakes. *Bull Seismol Soc Am* 92:230–244
- Gurbuz C, Ucer SB, Ozdemir H (1980) Adapazari yoresinde yapilan patlatma ile ilgili on degerlendirme sonuclari, reports on quarry blast recordings in the Adapazari Region. *Deprem Arastirma Bulteni* (in Turkish) 31:73–88
- Hanks TC, Kanamori H (1979) A moment magnitude scale. *J Geophys Res* 84:2348–2350
- Hartzell SH (1978) Earthquake Aftershocks as Green's Functions. *Geophys Res Lett* 5:1–4
- Horasan G, Gulen L, Pinar A, Kalafat D, Ozel N, Kuleli HS, Isikara AM (2002) Lithospheric structure of the Marmara and Aegean Regions, western Turkey. *Bull Seismol Soc Am* 92(1):322–329
- Hutchings L (1988) Modeling strong earthquake ground motion with an earthquake simulation program EMPYSYN that utilizes empirical Green's functions. Lawrence Livermore National Laboratory, Livermore, CA, p 122 (UCRL-ID-105890)
- Hutchings L (1991) "Prediction" of strong ground motion for the 1989 Loma Prieta earthquake using empirical Green's functions. *Bull Seismol Soc Am* 81:88–121
- Hutchings L (1994) Kinematic earthquake models and synthesized ground motion using empirical green's functions. *Bull Seismol Soc Am* 84:1028–1050
- Hutchings L (2004) Program NetMoment, a simultaneous inversion for moment, source corner frequency, and site specific t^* . Lawrence Livermore National Laboratory, Livermore. UCRL-ID 135693
- Hutchings L, Jarpe S (1996) Ground motion variability at the highways 14 and I-5 interchange in the Northern San Fernando Valley. *Bull Seis Soc Am* 86:S289–S299
- Hutchings L, Wu F (1990) Empirical Green's functions from small earthquakes: a waveform study of locally recorded aftershocks of the san fernando earthquake. *J Geophys Res* 95:1187–1214
- Hutchings L, Ioannidou E, Jarpe S, Stavrakakis GN (1997) Strong ground motion synthesis for a $M=7.2$ earthquake in the Gulf of Corinth, Greece using empirical Green's functions. Lawrence Livermore National Laboratory (UCRL-JC-129394)
- Hutchings L, Jarpe S, Kasameyer P (1998) Validation of a ground motion synthesis and prediction methodology for the 1988, $M=6.0$, sagueenay earthquake. Lawrence Livermore National Laboratory (UCRL-JC-129395)
- Hutchings L, Ioannidou E, Kalogeras I, Voulgaris N, Savy J, Foxall W, Scognamiglio L, Stavrakakis G (2007) A physically-based strong ground-motion prediction methodology; application to PSHA and the 1999 $M = 6.0$ Athens Earthquake. *Geophys J Int* 168:569–680
- Irikura K (1983) Semi-empirical estimation of strong ground motions during large earthquakes. *Bull Disaster Prev Res Inst Kyoto Univ* 33:63–104
- Jarpe SJ, Kasameyer PK (1996) Validation of a methodology for predicting broadband strong motion time histories using kinematic rupture models and empirical Green's functions. *Bull Seismol Soc Am* 86:1116–1129
- Kalkan E, Gulkan P, Yilmaz N, Celebi M (2009) Reassessment of probabilistic seismic hazard in the Marmara region. *Bull Seismol Soc Am* 99(4):2127–2146
- Karabulut H, Özalaybey S, Taymaz T, Aktar M, Selvi O, Kocaoğlu A (2003) A tomographic image of the shallow crustal structure in the Eastern Marmara. *Geophys Res Lett* 30(24):2777
- Kostrov BV (1964) Selfsimilar problems of propagating of shear cracks. *J Appl Math Mech (PMM)* 28:1077–1087
- Kuleli HS (1992) Three-dimensional modeling of the Aegean region with seismic tomography, Ph.D. thesis Istanbul Technical University, Istanbul (in Turkish)
- Kurtuluş Ç, Canbay MM (2007) Tracing the middle strand of the north Anatolian fault zone through the southern Sea of Marmara based on seismic reflection studies. *Geo Mar Lett* 27:27–40
- McClusky S et al (2000) Global Positioning System constraints on plate kinematics and dynamics in the eastern Mediterranean and Caucasus. *J Geophys Res* 105:5695–5719
- McKenzie DP (1972) Active tectonics of the Mediterranean region. *Geophys J R Astron Soc* 30:109–185
- Mert A, Pinar A, Fahjan Y, Hutchings L (2010) Prens adaları fayındaki depremlerin kaynak parametrelerinin eş zamanlı ve tekil ters çözüm teknikleri ile belirlenmesi. *İstanbul Yerbilimleri Dergisi* 23(1):53–63
- Mert A, Fahjan Y, Pinar A, Hutchings L (2011) İstanbul için tasarım esaslı kuvvetli yer hareketi dalga formlarının zaman ortamında türetilmesi. 1. Türkiye Deprem Mühendisliği ve Sismoloji Konferansı 11–14 Ekim 2011–ODTÜ – ANKARA
- Mert A, Fahjan Y, Pinar A, Hutchings L (2014a) Prens adaları fayında kuvvetli yer hareketi benzesimleri. *İMO Teknik Dergi*, Yazı 419:6775–6804
- Mert A, Fahjan Y, Pinar A, Hutchings L (2014b) Marmara Bölgesinde Ampirik Green Fonksiyon Yöntemiyle Deprem Benzeşimlerinin Elde Edilmesi. Hacettepe Üniversitesi Yerbilimleri Uygulama ve Araştırma Merkezi Bulteni, Yerbilimleri 35(1):55–78

- Nakamura A, Hasegawa A, Ito A, Ucer B, Baris S, Honkura Y, Kano T, Hori S, Pektas R, Komut T, Celik C, Isikara A (2002) P-wave velocity structure of the crust and its relationship to the Occurrence of the 1999 Izmit, Turkey, earthquake and Aftershocks. *Bull Seismol Soc Am* 92(1):330–338
- Örgülü G (2011) Seismicity and Source Parameters for small-scale earthquakes along the splays of the North Anatolian fault (NAF) in the Marmara Sea. *Geophys J Int* 184:385–404
- Papoulia J, Fahjan YM, Hutchings L, Novikova T (2015) PSHA for broad-band strong ground-motion hazards in the Saronikos Gulf, Greece, from potential earthquake with synthetic ground motion. *J Earthq Eng* 19:624–648
- Pınar A, Kuge K, Honkura Y (2003) Moment inversion of recent small to moderate sized earthquakes: implications for seismic hazard and active tectonics beneath the Sea of Marmara. *Geophys J Int* 153:133–145
- Pulido N, Ojeda A, Atakan K, Kubo T (2004) Strong ground motion estimation in the Sea of Marmara region (Turkey) based on a scenario earthquake. *Tectonophysics* 391:357–374
- Reilinger RE, McClusky SC, Oral MB, King MN, Toksoz MN, Barka A, Kinik I, Lenk O, Sanli I (1997) Global positioning system measurements of present-day crustal movements in the Arabia-Africa-Eurasia plate collision zone. *J Geophys Res* 102(B5):9983–9999
- Scognamiglio L, Hutchings L (2009) A test of physically based strong ground motion prediction methodology with the 26 September 1997, Mw = 6.0 Colfiorito (Umbria–Marche sequence), Italy earthquake. *Tectonophysics* 476:145–158
- Sengör AMC (1979) The North Anatolian transform fault: its age, offset and tectonic significance. *J Geol Soc* 136:263–282
- Somerville P, Irikura K, Graves R, Sawada S, Wald D, Abrahamson N, Kagawa YIT, Smith N, Kowada A (1999) Characterizing crustal earthquake slip models for the prediction of strong ground motion. *Seismol Res Lett* 70(1):59–80
- Sørensen BM, Pulido N, Atakan K (2007) Sensitivity of ground-motion simulations to earthquake source parameters: a case study for Istanbul, Turkey. *Bull Seismol Soc Am* 97(3):881–900
- Tanircan G (2012) İstanbul için 3 boyutlu hız modeli ile yer hareketi simülasyonu. *Gazi Üniversitesi Mühendislik Mimarlık Fakültesi Dergisi* 27(1):27–35
- Taymaz T, Jackson J, McKenzie D (1991) Active tectonics of the north and central Aegean Sea. *Geophys J Int* 106:433–490
- Wells DL, Coppersmith KJ (1994) New empirical relationships among magnitude, rupture length, rupture width, rupture area, and surface displacement. *Bull Seismol Soc Am* 84:974–1002
- Wennerberg L (1990) Stochastic summation of empirical Green's functions. *Bull Seismol Soc Am* 80:1418–1432
- Wössner J, Treml M, Wenzel F (2002) Simulation of M–W = 6.0 earthquakes in the Upper Rhinegraben using empirical Green functions. *Geophys J Int* 151(2):487–500
- Wu F (1978) Prediction of strong ground motion using small earthquakes, In: Proceedings of the 2nd international conference on microzonation, vol II. San Francisco, pp 701–704
- Yılmaz Y, Gökaşan E, Erbay AA (2009) Morphotectonic development of the Marmara region. *Tectonophysics*. <https://doi.org/10.1016/j.tecto.2009.05.012>
- Zor E, Ozalaybey S, Gurbuz C (2006) The crustal structure of the eastern Marmara region (Turkey) by teleseismic receiver functions. *Geophys J Int* 167:213–222